ACS ORGANIC & INORGANIC Au
AN OPEN ACCESS JOURNAL OF THE AMERICAN CHEMICAL SOCIETY

pubs.acs.org/orginorgau

Article

# Electrocatalytic Behavior of Tetrathiafulvalene (TTF) and Extended Tetrathiafulvalene (exTTF) [FeFe] Hydrogenase Mimics

Alejandro Torres, Alba Collado, Mar Gómez-Gallego, Carmen Ramírez de Arellano, and Miguel A. Sierra*

Cite This: *ACS Org. Inorg. Au* 2022, 2, 23–33

Read Online

ACCESS | Metrics & More | Article Recommendations | Supporting Information

**ABSTRACT:** TTF- and exTTF-containing $[(\mu\text{-}S_2)Fe_2(CO)_6]$ complexes have been prepared by the photochemical reaction of TTF or exTTF and $[(\mu\text{-}S_2)Fe_2(CO)_6]$. These complexes are able to interact with PAHs. In the absence of air and in acid media an electrocatalytic dihydrogen evolution reaction (HER) occurs, similarly to analogous $[(\mu\text{-}S_2)Fe_2(CO)_6]$ complexes. However, in the presence of air, the TTF and exTTF organic moieties strongly influence the electrochemistry of these systems. The reported data may be valuable in the design of [FeFe] hydrogenase mimics able to combine the HER properties of the [FeFe] cores with the unique TTF properties.

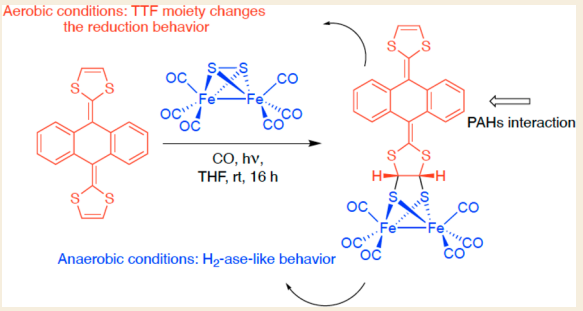


**KEYWORDS:** *Hydrogenase Mimics, TTF, exTTFs, Electrocatalysis, PAHs, π−π Interactions*

## INTRODUCTION

Hydrogenase enzymes are natural catalysts that promote the reversible transformation of protons into molecular hydrogen.[1−5] Among the three natural classes of hydrogenases, namely [FeFe] hydrogenases, [NiFe] hydrogenases, and [Fe] hydrogenases, the [FeFe] class shows an outstanding activity in hydrogen production.[6,7] It is not surprising that efforts to prepare simple nonprotein systems based on the main structural features of natural [FeFe] hydrogenases or related compounds have witnessed an explosive growth during the last 20 years.[7−12]

In this regard, derivatives of the $[(\mu\text{-}S_2)Fe_2(CO)_6]$ basic motif have been thoroughly studied for hydrogen production in the presence of an external electron donor.[7−13] The active site of [FeFe] hydrogenases (H-cluster) comprises a [2Fe] subcluster covalently linked via cysteine to a $[Fe_4S_4]$ cluster. Both sites are redox-active, and electron transfer is proton-coupled. The $[Fe_4S_4]$ cluster is a critical component that modulates the redox and catalytic properties of the H-cluster, acting as an electron injection site.[1−5]

Efforts to attach this critical component to a [FeFe] molecular model began with the incorporation of modified $[Fe_4S_4]$ clusters,[14] but more recent examples have used ferrocene,[15−18] maleic anhydride,[19] some bipyridine derivatives,[20] and $C_{60}$ fullerene derivatives[21] for this purpose. In fact, the only two examples of a [FeFe] mimic having a functional electron relay are the complex $[\mu\text{-}\{(SCH_2)_2NBn\}Fe_2(CO)_3(FcP^*)(dppv)]$ (**1**; FcP* = Cp*Fe-$(C_5Me_4CH_2PEt_2)$) (Figure 1) and its derivatives containing phosphole ligands coordinated to the [FeFe] center.[22,23] It is worth noting that among the plethora of [FeFe] hydrogenase mimics prepared, only these examples address the problem of attaching an electron relay (likely behaving as the "natural" $[Fe_4S_4]$ moiety).

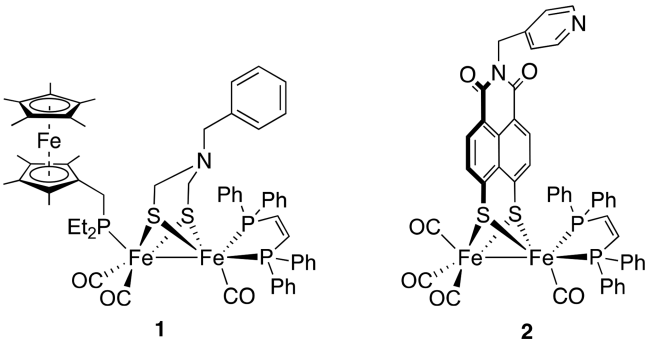


**Figure 1.** Examples of [FeFe] complexes bearing active redox moieties.

An alternative to the covalent attachment of the "electron reservoir" to the [FeFe] moiety is the use of systems such as **2** (Figure 1), which afford self-assembled entities in the presence of zinc tetraphenylporphyrin.[24] Several supramolecular struc-

Received: May 25, 2021
Published: September 13, 2021

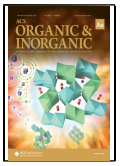

tures have been prepared, and their ability to promote electron transfer from the electron donor to the bimetallic catalytic moiety together with the photophysical properties of these systems has been studied.[13,24−27]

Tetrathiafulvalene (TTF) derivatives have been thoroughly studied in molecular and noncovalent chemistry because of their unique $\pi$-electron-donating properties.[28,29] The incorporation of TTF and extended tetrathiafulvalenes (exTTFs) as the donor moiety in donor−acceptor (D−A) systems is currently a well-established methodology in the building of organic-based materials with applications in different fields related to organic electronic devices.[30] In this regard, the oxidation of TTFs and exTTFs has been thoroughly and extensively studied because of their fundamental role in D−A organic molecules and devices.[28,29,31−35] The electrochemical oxidation of the neutral TTF shows two reversible and well-separated one-electron steps, which account for the formation of the radical cation and dicationic species, respectively.[36−40] These processes result in the intramolecular charge transfer (ICT) associated with the ground state of oxidized TTF derivatives.[41]

A less studied aspect of TTFs and exTTFs is their redox behavior in acid media and the role of the protonated TTF species in the reduction of $O_2$. The four-electron reduction of oxygen by TTF[42] in acidified dichloroethane and at the interface between two immiscible electrolyte solutions (ITIES) points to the relevant role of protonated TTF as the key species in the process. The selective reduction of $O_2$ and the reduction of protons by photoexcited $HTTF^+$ have been addressed in the presence of strong acid.[42,43] The protonation of the TTF is crucial for these reactions, and it is followed by the direct four-electron reduction of oxygen to water (Scheme 1).[42] In this regard, the production of $TTF^{\bullet+}$ was reported to

**Scheme 1. Reaction of TTF (3) with Oxygen in Acid Media**

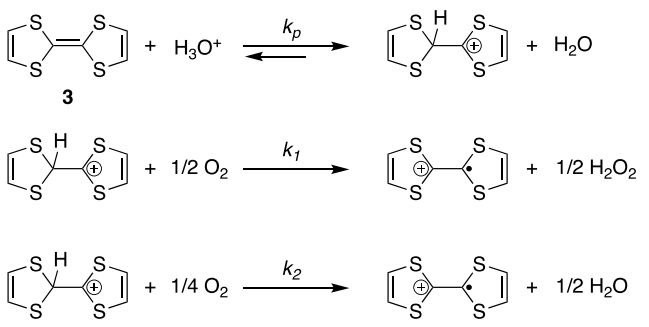


be much faster under aerobic conditions than that under anaerobic conditions. Also, protonated TTF-based molecules were indicated to be promising photoactivated redox shuttles for dihydrogen generation in the presence of metals.[44]

On the basis of these previous results, we were interested in studying the behavior of TTF (or exTTFs) when they are incorporated in a system that is designed for dihydrogen generation in the presence of acid. The combination of TTF and exTTFs with [FeFe] hydrogenase models is appealing, not only for their redox properties but also for their unique self-assembly properties and their ability to interact with planar polyaromatic hydrocarbons (PAHs) through $\pi-\pi$ interactions. These properties render them ideal candidates for the design of supramolecular models of [FeFe] hydrogenases able to interact with aromatic substrates or, by extension, with graphite or modified graphite surfaces.[31−35,45−48]

Reported herein are the synthesis and electrochemical properties of the first TTF-$[(\mu\text{-}S_2)Fe_2(CO)_6]$ and exTTF-$[(\mu\text{-}S_2)Fe_2(CO)_6]$ [FeFe] hydrogenase models. Our approach uses a mild photochemical procedure to incorporate the $[(\mu\text{-}S_2)Fe_2(CO)_6]$ moiety in sensitive substrates. NMR studies of the interaction of the prepared compounds and three simple PAHs will also be discussed.

## EXPERIMENTAL SECTION

### Materials and Methods

Unless otherwise stated, all of the reactions were carried out under Ar atmosphere using anhydrous solvents. The reaction workups were performed in air. $[(\mu\text{-}S_2)Fe_2(CO)_6]$,[49] 9,10-bis(1,3-dithiol-2-ylidene)-9,10-dihydroanthracene (**4**),[50] and 5,12-bis(1,3-dithiol-2-ylidene)-5,12-dihydronaphthacene (**5**)[51] were prepared according to the corresponding reported protocols. Complex **9** was prepared following literature procedures.[52] Commercially available tetrathiafulvalene (**3**) was used as received without further purification. $^1$H, $^{13}$C, and 2D COSY, HMQC, and HMBC NMR spectra were recorded at ambient temperature in $CDCl_3$ on a Bruker 500 MHz instrument; NOE spectra were recorded at 5 °C. Chemical shifts are expressed in parts per million and are referenced to residual solvent peaks ($^1$H, and $^{13}$C). ESI-HRMS was performed on an Agilent 6500 accurate mass spectrometer with a Q-TOF analyzer. Cyclic voltammograms were recorded using a Metrohm Model PGSTAT302N Autolab Potentiostat with a 3 mm glassy-carbon working electrode, Ag/AgCl 3 M as the reference electrode, and a 2 mm Pt-wire counter electrode. All of the measurements were performed at room temperature from $CH_3CN$ solutions containing $10^{-1}$ M $[NBu_4]PF_6$ as the supporting electrolyte, with analyte concentrations of $10^{-3}$ M. Unless otherwise stated, the experiments were carried out under an argon atmosphere.

### Computational Details

Geometry optimizations without symmetry constraints were carried out by using the Gaussian 16 suite of programs.[53] All calculations were performed at the DFT level by using the M06-2X functional[54−56] with an ultrafine integration grid.[57] Fe atoms were described by using the scalar relativistic Stuttgart−Dresden SDD pseudopotential[58] and its associated double-$\zeta$ basis set complemented with a set of f-polarization functions.[59] The 6-31G** basis set was used for the H, C, N, and O atoms.[60,61] All of the structures were fully optimized in $CH_3CN$ ($\varepsilon$ = 8.93) by using the SMD continuum model.[62]

### General Procedures for the Cycloadditions

In a Pyrex tube, $[(\mu\text{-}S_2)Fe_2(CO)_6]$ (1 equiv) and the corresponding tetrathiafulvalene (1 equiv) were dissolved in THF. The solution was bubbled with CO for 10 min, and the tube was sealed and irradiated (medium-pressure Hg lamp, 125 W, Pyrex filter, and Pyrex immersion well) for 16 h. After this time, the solvent was removed *in vacuo*, and the residue was purified by column chromatography.

**Compound 6.** By the general procedure with 50 mg of $[(\mu\text{-}S_2)Fe_2(CO)_6]$, and 30 mg of TTF (**3**) in 50 mL of THF as the starting materials, complex **6** was obtained as a red solid in 32% yield (25 mg) upon column chromatography ($SiO_2$, hexane). $^1$H NMR (500 MHz, $CDCl_3$): $\delta$ 6.28 (s, 2H), 4.94 (s, 2H) ppm. $^{13}$C NMR (126 MHz, $CDCl_3$): $\delta$ 207.1 (CO), 128.0 (C), 119.0 (CH), 108.8 (C), 70.0 (CH) ppm. IR (film): $\nu$(CO) 2084 (m), $\nu$(CO) 2033 (s), $\nu$(CO) 1993 (vs) cm$^{-1}$. HRMS-ESI: $m/z$ calcd for $C_{12}H_5Fe_2O_6S_6$ $[M + H]^+$ 548.71092, found $[M + H]^+$ 548.71150.

**Compound 7.** By the general procedure with 145 mg of complex $[(\mu\text{-}S_2)Fe_2(CO)_6]$, and 160 mg of exTTF **4** in 58 mL of THF as the starting materials, product **7** was obtained as an orange solid in 23% yield (69 mg) upon column chromatography ($SiO_2$, hexane/benzene 1/1). Complex **7** was obtained as a mixture of two conformers (7/3 ratio). $^1$H NMR (500 MHz, $CDCl_3$): $\delta$ 7.74 (d, $J$ = 7.7 Hz, 2H, *major*), 7.70 (d, $J$ = 7.6 Hz, 2H, *minor*), 7.51 (d, $J$ = 7.5 Hz, 2H,


https://doi.org/10.1021/acsorginorgau.1c00011
ACS Org. Inorg. Au 2022, 2, 23−33

*minor*), 7.41 (d, $J$ = 7.6 Hz, 2H, *major*), 7.36−7.24 (m, 4H, *major*; 4H, *minor*), 6.38 (s, 2H, *major*), 6.30 (s, 2H, *minor*), 5.01 (s, 2H, *major*), 4.66 (s, 2H, *minor*) ppm. $^{13}$C NMR (126 MHz, $CDCl_3$): $\delta$ 207.7 (br s, CO), 207.1 (br s, CO) 137.3 (C, *major*), 137.1 (C, *minor*), 136.7 (C, *major*), 136.5 (C, *minor*), 136.1 (C, *major*), 135.1 (C, *major*), 134.4 (C, *minor*), 133.1 (C, *minor*), 127.1 (CH, *major*), 126.9 (CH, *major, minor*), 126.8 (C, *minor*), 126.7 (CH, *major*), 126.4 (C, *major*), 126.0 (CH, *minor*), 126.0 (CH, *major*), 125.0 (CH, *major*), 125.0 (CH, *minor*), 121.6 (C, *major*), 121.5 (C, *minor*), 117.4 (CH, *major, minor*), 68.0 (CH, *major*), 67.5 (CH, *minor*) ppm. IR (film): $\nu$(CO) 2075 (s), $\nu$(CO) 2037 (vs), $\nu$(CO) 1993 (vs) cm$^{-1}$. HRMS-ESI: $m/z$ calcd for $C_{26}H_{13}Fe_2O_6S_6$ $[M + H]^+$ 724.77352, found $[M + H]^+$ 724.77290.

**Compound 8.** By the general procedure with 200 mg of complex $[(\mu\text{-}S_2)Fe_2(CO)_6]$ and 250 mg of exTTF **5** in 100 mL of THF as the starting materials, product **8** was obtained as an orange solid in 26% yield (116 mg) upon purification by column chromatography ($SiO_2$, hexane/benzene 1/1). Complex **8** was obtained as a mixture of two conformers (7:3 ratio). $^1$H NMR (500 MHz, $CDCl_3$): $\delta$ 8.06 (br s, 1H, *major*), 8.02 (br s, 1H, *minor*), 7.92−7.89 (m, 1H, *minor*), 7.84−7.80 (m, 3H, *major*), 7.77−7.76 (m, 1H, *major*, 2H, *minor*), 7.73 (d, $J$ = 7.6 Hz, 1H, *minor*), 7.50−7.43 (m, 3H, *major*, 3H, *minor*), 7.37−7.32 (m, 1H, *major*, 1H, *minor*), 7.30−7.26 (m, 1H, *major*, 1H, *minor*), 6.41 (ABq, $J$ = 6.8 Hz, 2H, *minor*), 6.33 (ABq, $J$ = 6.8 Hz, 2H, *minor*), 5.04 (ABq, $J$ = 7.2 Hz, 2H, *minor*), 4.62 (ABq, $J$ = 7.3 Hz, 2H, *minor*) ppm. $^{13}$C NMR (126 MHz, $CDCl_3$): $\delta$ 137.7 (C), 137.6 (C), 137.6 (C), 137.3 (C), 137.2 (C), 136.8 (C), 136.1 (C), 135.1 (C), 135.1 (C), 134.5 (C), 134.5 (C), 134.5 (C), 134.4 (C), 134.0 (C), 133.4 (C), 132.1 (C), 132.0 (C), 131.5 (C), 128.1 (CH), 127.8 (CH), 127.7 (CH), 127.4 (CH), 127.2 (CH), 127.1 (CH), 126.9 (CH), 126.8 (CH), 126.4 (CH), 126.4 (CH), 126.3 (CH), 126.2 (CH), 126.2 (CH), 126.2 (CH), 125.8 (CH), 125.3 (CH), 125.2 (CH), 125.2 (CH), 123.9 (CH), 123.8 (CH), 121.6 (C), 121.5 (C), 117.4 (CH), 117.4 (CH), 117.3 (CH), 67.9 (CH), 67.9 (CH), 67.5 (CH), 67.1 (CH) ppm. M−CO signals were not observed. IR (film): $\nu$(CO) 2076 (s), $\nu$(CO) 2038 (s), $\nu$(CO) 1998 (vs) cm$^{-1}$. HRMS-ESI: $m/z$ calcd for $C_{30}H_{15}Fe_2O_6S_6$ $[M + H]^+$ 774.78917, found $[M + H]^+$ 774.78596.

### Crystal data for compound 7 (major isomer):

$C_{26}H_{12}Fe_2O_6S_6$, $M_r$ = 724.42, triclinic, $a$ = 9.2289(5) Å, $b$ = 10.3173(6) Å, $c$ = 15.0606(8) Å, $\alpha$ = 91.047(2)°, $\beta$ = 90.335(2)°, $\gamma$ = 104.772(2)°, $V$ = 1386.32(13) Å$^3$, space group $P\bar{1}$, $Z$ = 2, $T$ = 120(2) K, $\lambda$ = 0.71073 Å, $D_{calcd}$ = 1.735 g cm$^{-3}$, $\mu$ = 1.540 cm$^{-1}$, 63127 reflections measured, 9784 unique ($R_{int}$ = 0.0549), red tablet obtained by $CH_2Cl_2$/*n*-pentane diffusion, crystal structure solved by dual-space methods with all non-hydrogen atoms refined anisotropically on $F^2$ using the programs SHELXT and SHELXL-2018,[63] hydrogen atoms included using a *riding* model, GOF = 1.105, $R(F_o, I > 2\sigma(I))$ = 0.0660, $R_w(F_o^2$, all data) = 0.1411.

## RESULTS AND DISCUSSION

Commercially available TTF (**3**) and the synthesized exTTFs **4** and **5** were employed in this study. Irradiation of TTF (**3**) and $[(\mu\text{-}S_2)Fe_2(CO)_6]$ in THF (medium-pressure Hg lamp, 125 W, Pyrex filter and Pyrex immersion well) for 16 h resulted in the formation of the photoadduct **6** (Scheme 2). Compound **6** was obtained as a pure compound in 32% yield after column chromatography, as a single *cis* diastereomer (see below).[64] Unreacted TTF and insoluble Fe residues were also obtained as byproducts, but the corresponding bis-adduct was not formed. The structure of the cycloadduct **6** was established on the basis of spectroscopic grounds. Especially relevant were the presence of a singlet at 4.94 ppm in the $^1$H NMR spectrum attributable to the ethylene bridge of the newly fused $[(\mu\text{-}S_2)Fe_2(CO)_6]$ ring, together with a signal at 207.1 ppm assignable to the CO ligands and the singlet of the newly formed CH at 70.0 ppm in the $^{13}$C NMR spectrum. All

**Scheme 2. Synthesis of TTF and exTTF $[(\mu\text{-}S_2)Fe_2(CO)_6]$ Derivatives 6−8**

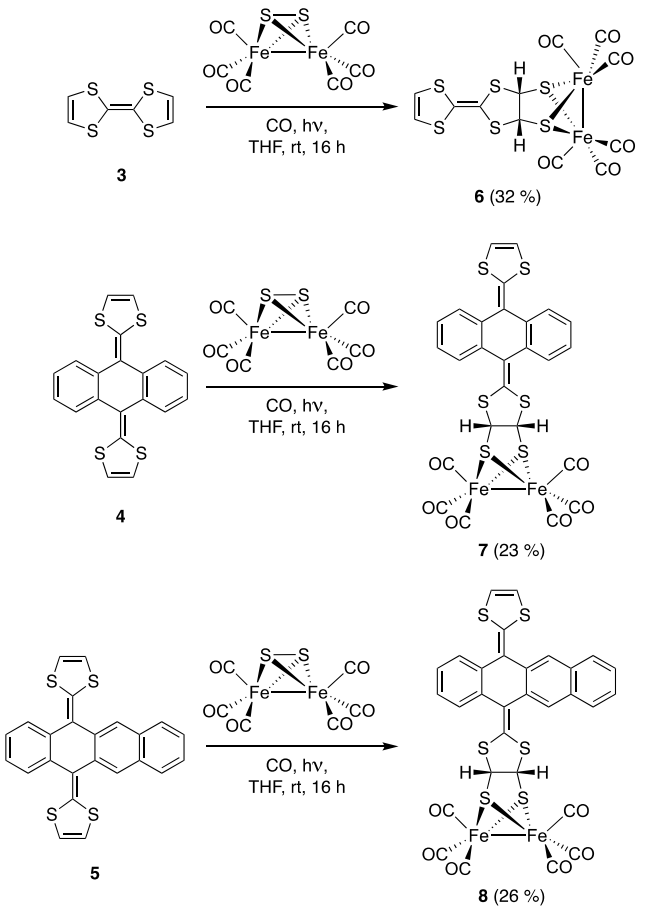


attempts to incorporate a second $[(\mu\text{-}S_2)Fe_2(CO)_6]$ moiety to complex **6** were unsuccessful.

Extended TTFs **4** and **5** were reacted next with $[(\mu\text{-}S_2)Fe_2(CO)_6]$ under conditions identical with those used to prepare complex **6**. Analogously, these reactions did not reach completion and compounds **7** and **8** were isolated in low yields (Scheme 2). The structures of compounds **7** and **8** deserve further discussion, as their NMR spectra revealed that they were obtained as a mixture of two conformational isomers in a 7/3 ratio (calculated by $^1$H NMR spectroscopy). This point was confirmed by variable-temperature $^1$H NMR experiments (DMSO-$d_6$) carried out with complex **7**. Thus, the signals at 6.81 ppm (major species) and 6.75 ppm (minor species), assignable to the vinylic protons, collapse into a broad signal at 6.74 ppm at 348 K (see Figure S42). The interconversion barrier for both conformers is $\Delta G^{\ddagger}_{348}$ = 18 kcal mol$^{-1}$. The structure of the major isomer was determined by an X-ray diffraction analysis (Figure 2). The conformational exchange could correspond to the rotation of the C(4)−C(15) bond. Figure 3 represents the computed structures of both conformers.

### Interaction of Compounds 6−8 with PAHs

The interaction of compounds **6**−**8** with three PAHs (anthracene, pyrene, and coronene; Figures S18−S26) was studied next by $^1$H NMR spectroscopy. Figure 4 shows the titration experiment of compound **7** with pyrene (1−14 equiv) as a representative example. The shielding of the signal of the $S_2CH$−$CHS_2$ protons of the minor conformer was clearly


https://doi.org/10.1021/acsorginorgau.1c00011
ACS Org. Inorg. Au 2022, 2, 23−33

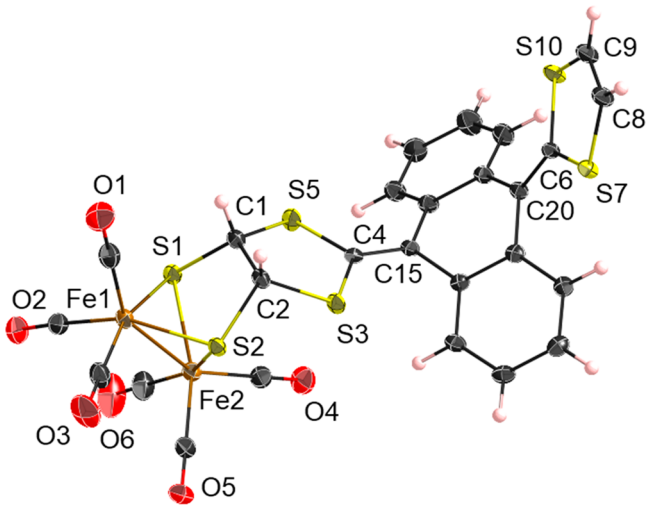


**Figure 2.** X-ray thermal ellipsoid plot for the major isomer of compound **7** (50% probability level). Selected bond lengths (Å) and angles (deg): Fe(1)−Fe(2) 2.5184(8), Fe(1)−S(1) 2.2469(10), Fe(1)−S(2) 2.2304(10), Fe(2)−S(1) 2.2335(10), Fe(2)−S(2) 2.2257(11), C(1)−C(2) 1.528(5), C(4)−C(15) 1.352(5), S(2)−Fe(1)−S1 80.30(4), S(2)−Fe(2)−S(1) 80.69(4), C(15)−C(4)−S(3) 122.1(3), C(15)−C(4)−S(5) 124.3(3), S(3)−C(4)−S(5) 113.53(19), C(4)−C(15)−C(22) 124.5(3), C(4)−C(15)−C(21) 121.6(3), C(22)−C(15)−C(21) 113.8(3).

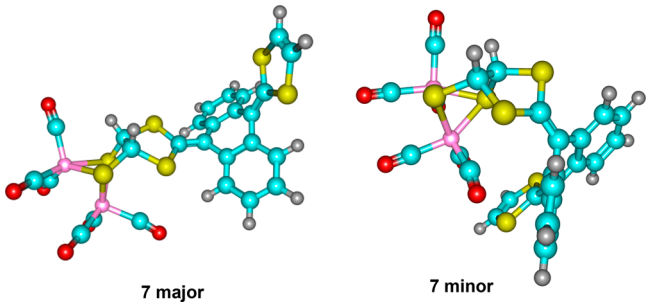


**Figure 3.** Computed structures of both conformers of complex **7**. Exchange barrier (experimental): $\Delta G^{\ddagger}_{348}$ = 18 kcal mol$^{-1}$. Calculations were carried out at the M062X-D3-6-31G**-SDD, $CH_3CN$-SMD level; see the Supporting Information for additional data.

observed (∼0.1 ppm), whereas for the major conformer, the signal shielding is slightly lower (∼0.08 ppm). Analogous results were observed for complex **8** (Figure S24).

A similar study with anthracene (up to 10 equiv) showed a small shielding of the $S_2CH-CHS_2$ signals of the minor isomers (∼0.015 ppm for **7** and ∼0.05 ppm for **8**), whereas in the case of coronene, the shielding effect is more visible in the signals of the major isomers of both complexes (see Figures S22, S23, S25, and S26). These experimental data suggest a relevant influence of the structure of the PAH in the interaction with the complex. The interaction of complex **6** with PAHs shows small signal shifts (<0.05 ppm) in the NMR studies (see Figures S18−S20). These experiments show that complexes **6**−**8** interact with PAHs in solution, which indicates that they may be good candidates for the study of interaction of [FeFe] hydrogenase mimics with aromatic surfaces.

## Electrochemistry

The electrochemical behavior of complexes **6**−**8** was studied next (Figure 5 and Table 1). Complex **6**, lacking aromatic groups, shows an intense irreversible reduction wave at −1.53 V and two quasi-reversible events at −1.82 and −2.10 V. In oxidation, a reversible wave, characteristic of the TTF moiety, is observed at 0.26 V (Figure 5 and Figure S1).

Complexes **7** and **8**, derived from exTTFs, present a similar electrochemical behavior. Their cyclic voltammograms show a quasi-reversible reduction waves at −1.52 and −1.47 V and reversible oxidation waves at 0.19 and 0.33 V, respectively, attributable to the exTTF fragment (Figure 5 and Figures S4 and S7).[65]

The shift in the cathodic potential with the scan rate ($\delta E_{pc}/\delta \ln \nu$) (Figure 6) allowed the calculation of the number of electrons that participate in the reduction event. As shown in eq 1, the experimental value (25.6 mV) indicated a one-electron process:[23]

$$\frac{\partial E}{\partial \ln \nu} = \frac{RT}{nF} = -25.6 \text{ mV when } n = 1 \quad (1)$$

There is a clear difference in the electrochemical behavior observed for the TTF-derived complex **6** and the exTTF complexes **7** and **8**, which can be explained by an analysis of the distribution of their LUMO orbitals (Figure 7).[66−70] Thus, while the LUMO of complex **6** is centered on the $[(\mu\text{-}S_2)Fe_2(CO)_6]$ fragment, the LUMOs of complexes **7** and **8** (major isomers) are distributed along the exTTF moieties. Hence, the reduction of complex **6** should involve the $[(\mu\text{-}S_2)Fe_2(CO)_6]$ moiety, which is known to undergo two successive $[Fe^IFe^I]/[Fe^0Fe^I]$ and $[Fe^0Fe^I]/[Fe^0Fe^0]$ reduction processes.[71−73] In contrast, exTTF derivatives **7** and **8** would first experience reduction on the exTTF fragment rather than reduction of the bimetallic moiety. The process should generate an extended radical anion, species involved in the successive redox processes.

The electrochemistry of complexes **6**−**8** in acid media was studied next. These complexes did not show electrocatalytic behavior at the first reduction level in the presence of increasing amounts of acetic acid ($pK_a \approx 22.3$ in $CH_3CN$)[74] (up to 20 equiv), but a peak appears at around −2.25 V whose intensity grows with the acid concentration (see Figure 8 and Figures S2 and S5; see Figures S9 and S10 for blank experiments). This behavior is compatible with two successive reduction processes followed by electrocatalytic production of $H_2$ by the species formed in the second reduction event.[67,75−77] The CV in Figure 8 also shows the appearance of a peak at about −1.2 V that increases with an increase in the amount of AcOH. The origin of this new wave is at this moment unknown.

In the presence of a stronger acid, $HBF_4$, there is a significant electrocatalytic response in the first reduction event in all of the cases (Figure 9, Figures S3 and S6, and Table 2). Increasing the acid concentration up to 3.8 mol equiv leads to an average current increase in this reduction wave of 300% (Figure 10; see Figures S11 and S12 for blank experiments).[78] The current height of this wave increases linearly with the concentration of acid, and the plots of $i_{cat}/i_p$ versus the $HBF_4$ concentration show different sensitivities of the complexes to the acid concentration, compound **8** (having the most conjugated exTTF spacer) being the least sensitive (Figure 10). At a high concentration of $HBF_4$ a new electrochemical event is observed at −0.93 V in **7** and **8**. This new wave could be attributable to the reduction of a protonated form of the complexes in the distal C=C bond (with respect to the $[(\mu\text{-}S_2)Fe_2(CO)_6]$ fragment) of the TTF moiety.[79] The generation


https://doi.org/10.1021/acsorginorgau.1c00011
ACS Org. Inorg. Au 2022, 2, 23−33

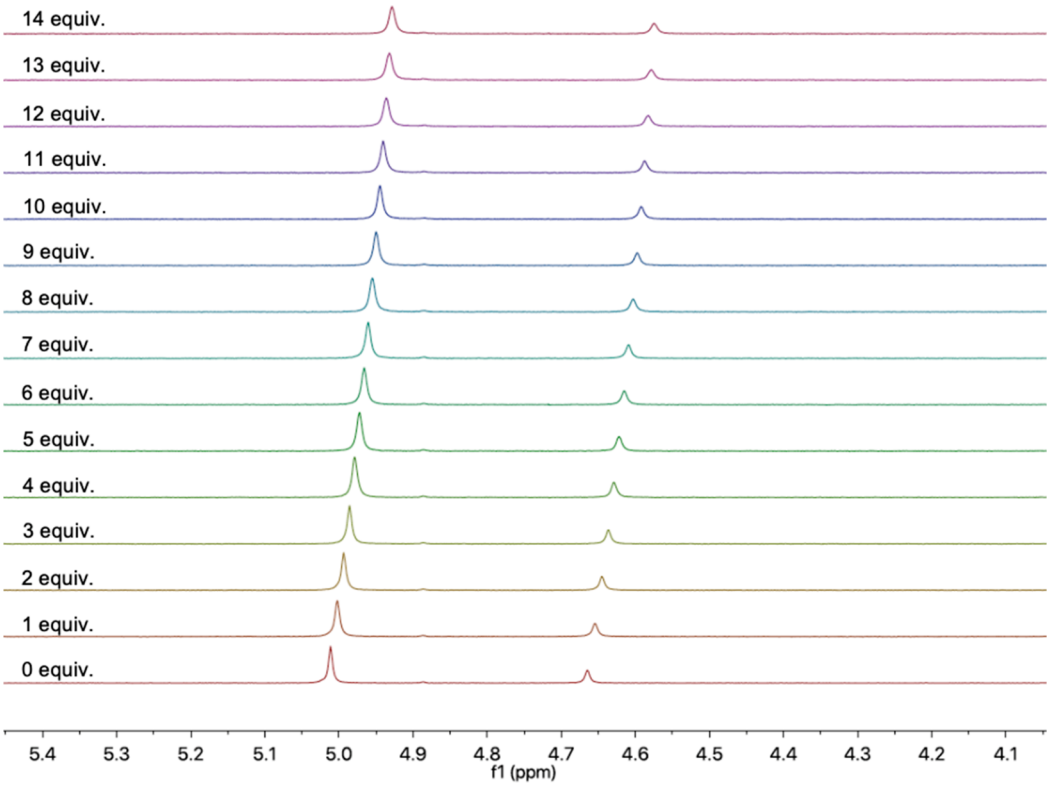


**Figure 4.** $^1$H NMR ($CDCl_3$) spectra of complex **7** and increasing amounts (1−14 equiv) of pyrene.

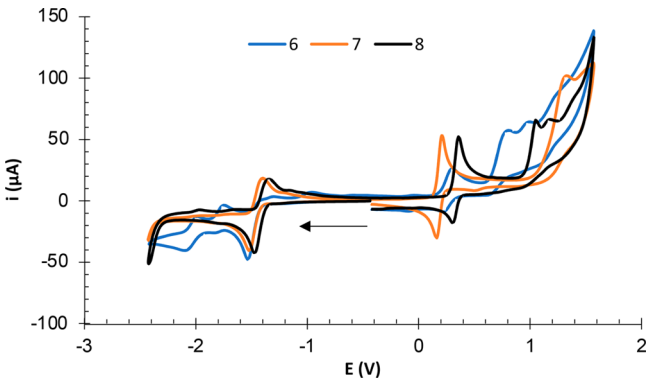


**Figure 5.** Cyclic voltammograms (CVs) of complexes **6**−**8**. Data were obtained from $10^{-3}$ M $CH_3CN$ solutions containing $10^{-1}$ M $[NBu_4]PF_6$ as the supporting electrolyte at 25 °C: counter electrode, Pt; working electrode, glassy carbon; potentials given in V vs $Fc^+/Fc$; scan rate, 100 mV/s.

**Table 1. Electrochemical Data of Compounds 6−8**[a]

| | reduction | | | |
|---|---|---|---|---|
| complex | $E_{pc}$ | $E_{pa}$ | $E_{1/2}$ | oxidation $E_{1/2}$ |
| **6** | −1.53 | −0.96 | −1.79 | 0.26 |
| | −1.82 | −1.75 | −2.05 | |
| | −2.10 | −1.99 | | |
| **7** | −1.52 | −1.40 | −1.46 | 0.19 |
| **8** | −1.47 | −1.34 | −1.41 | 0.33 |

[a]Data in V vs $Fc^+/Fc$; scan rate ($\nu$) 100 mV/s.

of a protonated species in the strong acid medium was confirmed by $^1$H NMR experiments of complex **7** in the

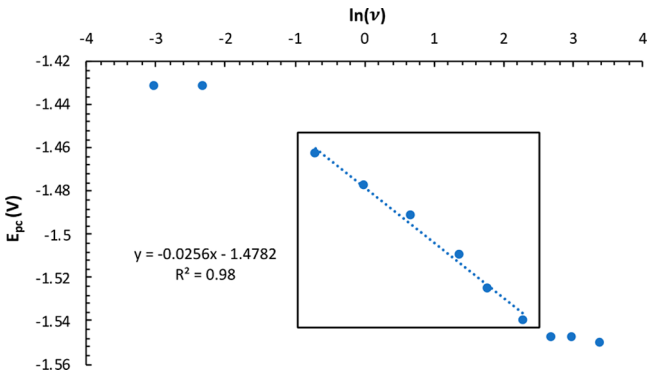


**Figure 6.** $E_{pc}$ versus ln $\nu$ for complex **8**. The purely kinetic region is shown inside the black square.

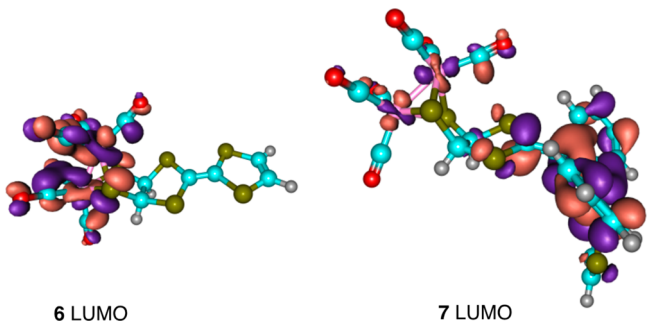


**Figure 7.** Distribution of the LUMOs of complexes **6** and **7**. Calculations were carried out at the M062X-D3-6-31G**-SDD,$CH_3CN$ -SMD level; see the Supporting Information for additional data.



https://doi.org/10.1021/acsorginorgau.1c00011
ACS Org. Inorg. Au 2022, 2, 23−33

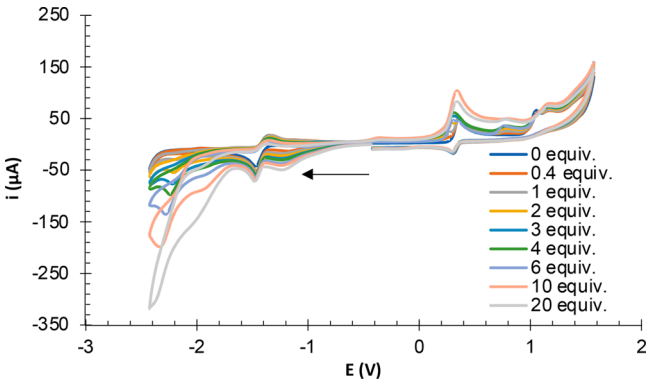


**Figure 8.** Cyclic voltammograms of a $CH_3CN$ solution of compound **8** ($10^{-3}$ M) with HOAc (0–20 equiv of $H^+$) containing $10^{-1}$ M $[NBu_4]PF_6$ as the supporting electrolyte at 25 °C: counter electrode, Pt; working electrode, glassy carbon; potentials given in V vs $Fc^+/Fc$; scan rate, 100 mV/s.

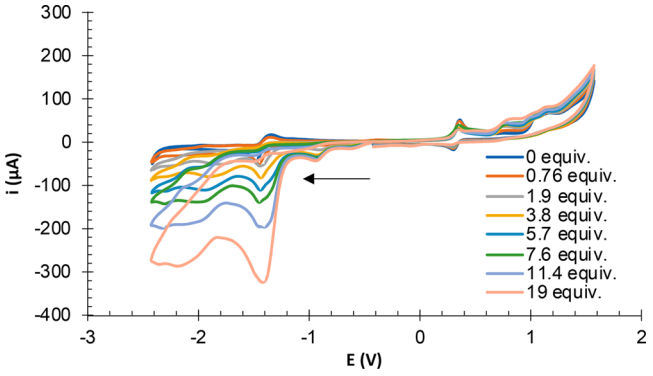


**Figure 9.** Cyclic voltammograms of a $CH_3CN$ solution of compound **8** ($10^{-3}$ M) with $HBF_4{\cdot}Et_2O$ (0–19 equiv of $H^+$) containing $10^{-1}$ M $[NBu_4]PF_6$ as the supporting electrolyte at 25 °C: counter electrode, Pt; working electrode, glassy carbon; potentials given in V vs $Fc^+/Fc$; scan rate, 100 mV/s.

**Table 2. Electrochemical Data for Complexes 6–8 in the Presence of $HBF_4{\cdot}Et_2O$[a]**

| | 6 | 7 | 8 |
|---|---|---|---|
| $E_{cat}$[b,81] | −1.53 | −1.49 | −1.45 |
| $\eta$[c] | −1.25 | −1.21 | −1.17 |
| TOF[d] | 5.9 | 3.4 | 1.2 |
| $TOF_{max}$[e] | 5.9 | 13.7 | 11.0 |

[a]Data in V vs $Fc^+/Fc$. [b]Data taken from Figures 9, S3 and S6. [c]Overpotential ($\eta$) was calculated using $E°_{HA}$ = −0.28 V.[81] [d]TOF values in $s^{-1}$ were calculated at 5.7 mM $HBF_4{\cdot}Et_2O$.[82] [e]$TOF_{max}$ values in $s^{-1}$ were calculated at the highest acid concentration tolerated by each complex (5.7 mM for **6**, 11.4 mM for **7**, and 19 mM for **8**).

presence of variable amounts of $HBF_4$ (see Figures S43–S45).[80]

Being aware of the redox reactivity of TTF in acid media (see above),[42−44] we necessarily had to consider the contribution of electrochemical reactions due to the TTF moieties in the above processes. In this regard, we decided to synthesize the well-known [FeFe] complex **9**, which could serve as a model for this study, since it contains the [FeFe] center but lacks the TTF or exTTF moiety. Complex **9** was prepared (45% yield) following literature procedures by the reaction of the commercially available benzene-1,2-dithiol with

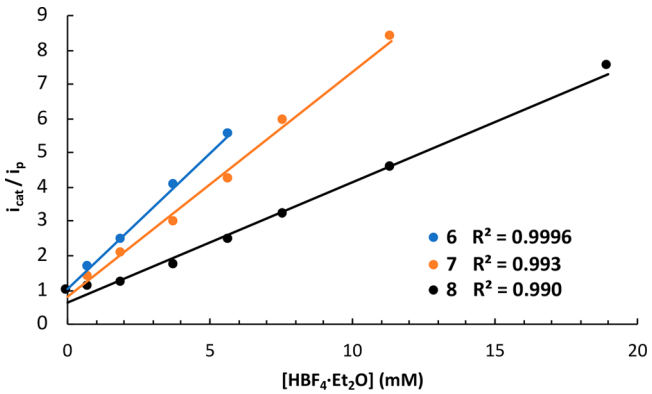


**Figure 10.** Plots of $i_{cat}/i_p$ as a function of $HBF_4{\cdot}Et_2O$ concentration for complexes **6–8**.

$Fe_2(CO)_9$ (Scheme 3),[52] and its electrochemical behavior was recorded.

**Scheme 3. Synthesis of Complex 9**

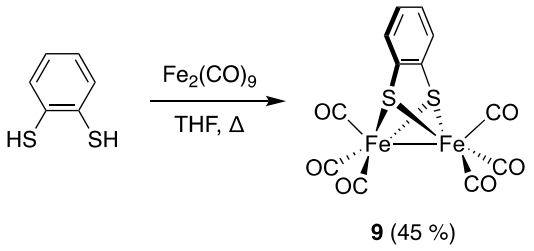


The study of the electrochemical response of model complex **9** under an anaerobic atmosphere (Figure 11) shows a

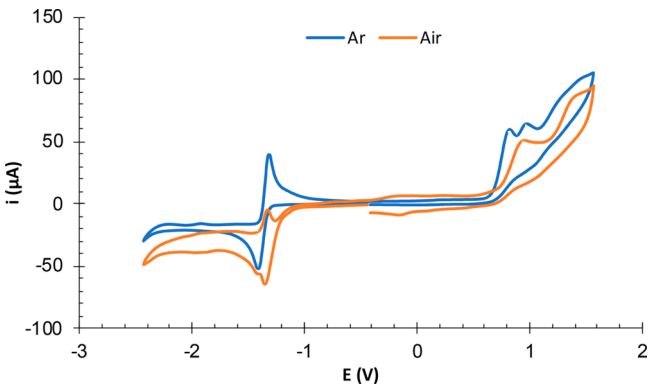


**Figure 11.** Comparison of cyclic voltammograms of complex **9** under Ar and in air. The wave at −1.41 V corresponds to the formation of dianion $\mathbf{9}^{2-}$. The process at −1.35 V is due to $O_2$ (Figure S16). Data were obtained from $10^{-3}$ M $CH_3CN$ containing $10^{-1}$ M $[NBu_4]PF_6$ as the supporting electrolyte at 25 °C: counter electrode, Pt; working electrode, glassy carbon; potentials given in V vs $Fc^+/Fc$; scan rate, 100 mV/s.

behavior compatible with the electrochemistry of the [FeFe] moiety, with the characteristic two-electron reduction wave at −1.41 V corresponding to the formation of dianion $\mathbf{9}^{2-}$.[70,83−86] This wave experienced changes when air was bubbled in the solution (Figure 11). A similar behavior was observed when the experiment was performed in the presence of $HBF_4$ (Figure S14). The reactivity of [FeFe] hydrogenases with $O_2$ has been


https://doi.org/10.1021/acsorginorgau.1c00011
ACS Org. Inorg. Au 2022, 2, 23−33

extensively studied.[87−91] In the case of [FeFe] hydrogenase mimics, recent work points to a relationship between the reactivity with molecular oxygen and the structure of the [FeFe] bridge, the azadithiolate (adt) derivatives being very reactive whereas the propanedithiolate (pdt) derivatives exhibit reduced reactivity.[90] The results in Figure 11 show that **9**, having a benzenedithiolate (bdt) bridge, is also reactive toward $O_2$. Nevertheless, additional reduction events were not observed when the cyclic voltammetry of **9** was recorded in air.

Analogous experiments were carried out with the exTTF-[FeFe] complex **8**. Figure 12 and Figure S15 show the

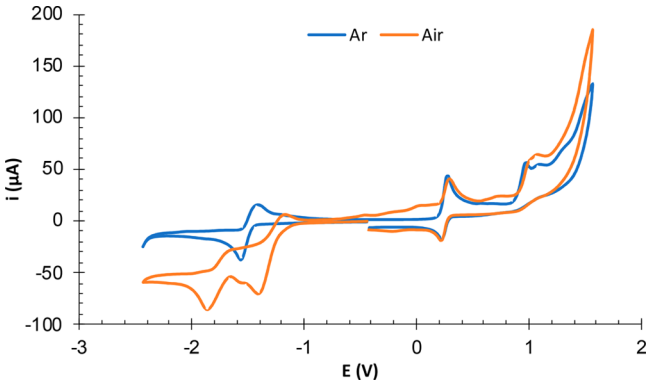


**Figure 12.** Cyclic voltammograms of complex **8** under Ar and in air. The first reduction wave (orange CV) corresponds to the presence of oxygen. Data were obtained from $10^{-3}$ M $CH_3CN$ containing $10^{-1}$ M $[NBu_4]PF_6$ as the supporting electrolyte at 25 °C: counter electrode, Pt; working electrode, glassy carbon; potentials given in V vs $Fc^+/Fc$; scan rate, 100 mV/s.

voltammograms under Ar and in the presence of $O_2$. In contrast to what was observed for complex **9**, in an aerated solution (Figure 11), in addition to the wave attributable to the reduction of the [FeFe] moiety at −1.47 V, a new reduction wave appears at −1.86 V. On consideration of the results with model complex **9** (see above), this new wave should be attributable to the presence of the exTTF moiety.

An analysis of the experiments above and the data in Figures 11 and 12 suggest that, as for complex **9**, the electrochemical responses of TTF and exTTF-[FeFe] complexes **6**−**8** in acid media ($HBF_4{\cdot}Et_2O$) under an inert atmosphere can be interpreted as a consequence of their hydrogenase-like behavior (see also Figures 8 and 9 and Figures S1−S7), not from redox processes due to the TTF moieties. However, in the presence of air, TTF and exTTF substituents clearly influence the redox behavior of these complexes (see Figure 12).[42,92]

A computational study of the orbitals of the protonated species sheds more light on the electrochemical behavior of complexes **6**−**8** with $HBF_4$ in the absence of air. As shown in Figure 13, protonation of TTF and exTTF in **6** and **7** should facilitate the reduction of the molecule and thence the catalytic activity of the [FeFe] cluster. In fact, the LUMOs of $\mathbf{6H^+}$ and $\mathbf{7H^+}$ as well as the SOMOs of their reduced species ($\mathbf{6H^{\bullet+}}$ and $\mathbf{7H^{\bullet+}}$) are mainly controlled by the TTF and exTTF fragments.

## CONCLUSIONS

To conclude, new types of TTF-containing $[(\mu\text{-}S_2)Fe_2(CO)_6]$ complexes showing [FeFe] hydrogenase-like behavior have been prepared and their electrochemical and electrocatalytic

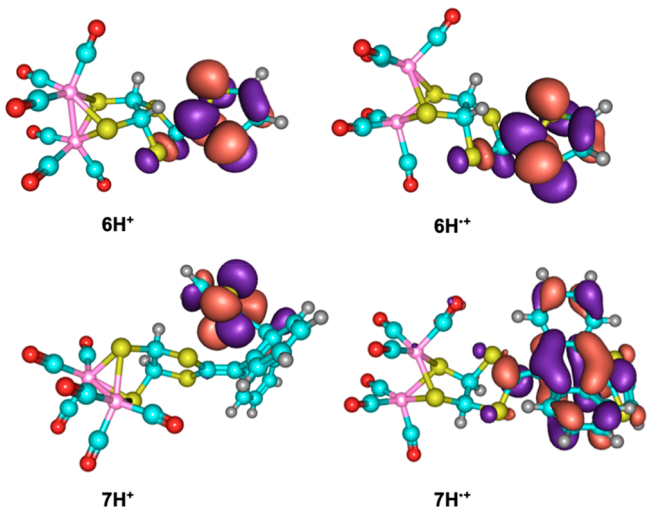


**Figure 13.** Computed (M062X-D3-6-31G**-SDD,$CH_3CN$-SMD) LUMOs of $\mathbf{6H^+}$ and $\mathbf{7H^+}$ and SOMOs of $\mathbf{6H^{\bullet+}}$ and $\mathbf{7H^{\bullet+}}$ (see the Supporting Information for additional data).

properties, as well as their interaction with PAHs, studied. Complexes with exTTF structures are able to interact with PAHs, the interaction degree depending on the structure of the PAH. Due to their electroactive nature, the incorporation of the TTF and exTTF fragments in complexes **6**−**8** modifies their usual behavior in reduction. In acidic anaerobic media a clear electrocatalytic reaction, typical of dihydrogen evolution (HER), occurs. However, under aerobic conditions the presence of TTF and exTTF moieties strongly influences the electrochemical behavior of complexes **6**−**8**. This has been demonstrated by carrying out different electrochemical experiments in the presence and in the absence of air, as well as by comparison of complexes **6**−**8** with the structurally related complex **9**, lacking the electroactive TTF moieties. Work to translate the results of this study to the design of supramolecular models of [FeFe] hydrogenases able to interact with aromatic or modified graphite surfaces is underway in our laboratories.

## ASSOCIATED CONTENT

### Supporting Information

The Supporting Information is available free of charge at https://pubs.acs.org/doi/10.1021/acsorginorgau.1c00011.

Full characterization of complexes **6**−**8**, X-ray data for complex **7**, computational details, and full electrochemical data for all of the experiments discussed in this work (PDF)

### Accession Codes

CCDC 2012973 contains the supplementary crystallographic data for this paper. These data can be obtained free of charge via www.ccdc.cam.ac.uk/data_request/cif, or by emailing data_request@ccdc.cam.ac.uk, or by contacting The Cambridge Crystallographic Data Centre, 12 Union Road, Cambridge CB2 1EZ, UK; fax: +44 1223 336033.

## AUTHOR INFORMATION

### Corresponding Author

**Miguel A. Sierra** − *Departamento de Química Orgánica I, Facultad de Química, Universidad Complutense, 28040*



https://doi.org/10.1021/acsorginorgau.1c00011
ACS Org. Inorg. Au 2022, 2, 23−33

*Madrid, Spain; Center for Innovation in Advanced Chemistry (ORFEO-CINQA), Facultad de Química, Universidad Complutense, 28040 Madrid, Spain;* orcid.org/0000-0002-3360-7795; Email: sierraor@ucm.es

## Authors

**Alejandro Torres** − *Departamento de Química Orgánica I, Facultad de Química, Universidad Complutense, 28040 Madrid, Spain; Center for Innovation in Advanced Chemistry (ORFEO-CINQA), Facultad de Química, Universidad Complutense, 28040 Madrid, Spain;* orcid.org/0000-0001-6767-7137

**Alba Collado** − *Departamento de Química Orgánica I, Facultad de Química, Universidad Complutense, 28040 Madrid, Spain; Center for Innovation in Advanced Chemistry (ORFEO-CINQA), Facultad de Química, Universidad Complutense, 28040 Madrid, Spain;* Present Address: Departamento de Quimica Inorgánica, Universidad Autónoma de Madrid, C/Francisco Tomás y Valiente, 7. Crta. Colmenar, km. 15, 28049 Madrid, Spain; orcid.org/0000-0001-6215-1822

**Mar Gómez-Gallego** − *Departamento de Química Orgánica I, Facultad de Química, Universidad Complutense, 28040 Madrid, Spain; Center for Innovation in Advanced Chemistry (ORFEO-CINQA), Facultad de Química, Universidad Complutense, 28040 Madrid, Spain;* orcid.org/0000-0002-8961-7685

**Carmen Ramírez de Arellano** − *Center for Innovation in Advanced Chemistry (ORFEO-CINQA), Facultad de Química, Universidad Complutense, 28040 Madrid, Spain; Departamento de Química Orgánica, Universidad de Valencia, 46100 Valencia, Spain*

Complete contact information is available at: https://pubs.acs.org/10.1021/acsorginorgau.1c00011

## Author Contributions

The manuscript was written through contributions of all authors. The paper was designed and written with contributions of all authors. C.R.d.A. determined the X-ray structure of complex **7** and wrote the structural discussion.

## Notes

The authors declare no competing financial interest.

## ■ ACKNOWLEDGMENTS

Support for this work under grants PID2019-108429RB-I00 and RED2018-102387-T from the MCI (Spain) is gratefully acknowledged. M.A.S. thanks the Fundación Ramón Areces for a grant from the XVIII Concurso Nacional de Ayudas a la Investigación en Ciencias de la Vida y de la Materia (CIVP18A3938). A.C. thanks the MINECO (Spain) for a Juan de la Cierva-Incorporación Fellowship.

## ■ REFERENCES

(1) Lubitz, W.; Ogata, H.; Rüdiger, O.; Reijerse, E. Hydrogenases. *Chem. Rev.* **2014**, *114*, 4081−4148.
(2) Vignais, P. M.; Billoud, B. Occurrence, Classification, and Biological Function of Hydrogenases: An Overview. *Chem. Rev.* **2007**, *107*, 4206−4272.
(3) Rodríguez-Maciá, P.; Kertess, L.; Burnik, J.; Birrell, J. A.; Hofmann, E.; Lubitz, W.; Happe, T.; Rüdiger, O. His-Ligation to the [4Fe-4S] Subcluster Tunes the Catalytic Bias of [FeFe] Hydrogenase. *J. Am. Chem. Soc.* **2019**, *141*, 472−481.
(4) Esmieu, C.; Guo, M.; Redman, H. J.; Lundberg, M.; Berggren, G. Synthesis of a Miniaturized [FeFe] Hydrogenase Model System. *Dalton Trans.* **2019**, *48*, 2280−2284.
(5) Senger, M.; Mebs, S.; Duan, J.; Shulenina, O.; Laun, K.; Kertess, L.; Wittkamp, F.; Apfel, U.-P.; Happe, T.; Winkler, M.; Haumann, M.; Stripp, S. T. Protonation/Reduction Dynamics at the [4Fe−4S] Cluster of the Hydrogen-Forming Cofactor in [FeFe]-Hydrogenases. *Phys. Chem. Chem. Phys.* **2018**, *20*, 3128−3140.
(6) Frey, M. Hydrogenases: Hydrogen-Activating Enzymes. *ChemBioChem* **2002**, *3*, 153−160.
(7) Wittkamp, F.; Senger, M.; Stripp, S. T.; Apfel, U. P. [FeFe]-Hydrogenases: Recent Developments and Future Perspectives. *Chem. Commun.* **2018**, *54*, 5934−5942.
(8) Kleinhaus, J. T.; Wittkamp, F.; Yadav, S.; Siegmund, D.; Apfel, U.-P. [FeFe]-Hydrogenases: Maturation and Reactivity of Enzymatic Systems and Overview of Biomimetic Models. *Chem. Soc. Rev.* **2021**, *50*, 1668−1784.
(9) Ahmed, M. E.; Dey, A. Recent Developments in Bioinspired Modelling of [NiFe]- and [FeFe]-Hydrogenases. *Curr. Opin. Electrochem.* **2019**, *15*, 155−164.
(10) Schilter, D.; Camara, J. M.; Huynh, M. T.; Hammes-Schiffer, S.; Rauchfuss, T. B. Hydrogenase Enzymes and Their Synthetic Models: The Role of Metal Hydrides. *Chem. Rev.* **2016**, *116*, 8693−8749.
(11) Apfel, U.-P.; Pétillon, F. Y.; Schollhammer, P.; Talarmin, J.; Weigand, W. [FeFe] Hydrogenase Models: an Overview. In *Bioinspired Catalysis: Metal-Sulfur Complexes*; Weigand, W., Schollhammer, P., Eds.; Wiley-VCH: 2014; Chapter 4.
(12) Simmons, T. R.; Berggren, G.; Bacchi, M.; Fontecave, M.; Artero, V. Mimicking Hydrogenases: From Biomimetics to Artificial Enzymes. *Coord. Chem. Rev.* **2014**, *270*−*271*, 127−150.
(13) Nurttila, S. S.; Becker, R.; Hessels, J.; Woutersen, S.; Reek, J. N. H. Photocatalytic Hydrogen Evolution by a Synthetic [FeFe] Hydrogenase Mimic Encapsulated in a Porphyrin Cage. *Chem. - Eur. J.* **2018**, *24*, 16395−16406 and the pertinent references therein..
(14) Tard, C.; Liu, X.; Ibrahim, S. K.; Bruschi, M.; Gioia, L. D.; Davies, S. C.; Yang, X.; Wang, L.-S.; Sawers, G.; Pickett, C. J. Synthesis of the H-Cluster Framework of Iron-Only Hydrogenase. *Nature* **2005**, *433*, 610−613.
(15) Zeng, X.; Li, Z.; Xiao, Z.; Wang, Y.; Liu, X. Using Pendant Ferrocenyl Group(S) as an Intramolecular Standard to Probe the Reduction of Diiron Hexacarbonyl Model Complexes for the Sub-Unit of [FeFe]-Hydrogenase. *Electrochem. Commun.* **2010**, *12*, 342−345.
(16) Liu, Y.-C.; Lee, C.-H.; Lee, G.-H.; Chiang, M.-H. Influence of a Redox-Active Phosphane Ligand on the Oxidations of a Diiron Core Related to the Active Site of Fe-Only Hydrogenase. *Eur. J. Inorg. Chem.* **2011**, *2011*, 1155−1162.
(17) Gimbert-Suriñach, C.; Bhadbhade, M.; Colbran, S. B. Bridgehead Hydrogen Atoms Are Important: Unusual Electrochemistry and Proton Reduction at Iron Dimers with Ferrocenyl-Substituted Phosphido Bridges. *Organometallics* **2012**, *31*, 3480−3491.
(18) Zhao, J.; Wei, Z.; Zeng, X.; Liu, X. Three Diiron Complexes Bearing an Aromatic Ring as Mimics of the Diiron Subunit of [FeFe]-Hydrogenase: Synthesis, Electron Transfer and Coupled Chemical Reactions. *Dalton Trans.* **2012**, *41*, 11125−11133.
(19) Si, Y.; Charreteur, K.; Capon, J.-F.; Gloaguen, F.; Pétillon, F. Y.; Schollhammer, P.; Talarmin, J. Non-Innocent Bma Ligand in a Dissymetrically Disubstituted Diiron Dithiolate Related to the Active Site of the [FeFe] Hydrogenases. *J. Inorg. Biochem.* **2010**, *104*, 1038−1042.
(20) Roy, S.; Groy, T. L.; Jones, A. K. Biomimetic Model for [FeFe]-Hydrogenase: Asymmetrically Disubstituted Diiron Complex with a Redox-Active 2,2′-Bipyridyl Ligand. *Dalton Trans.* **2013**, *42*, 3843−3853.
(21) Liu, Y.-C.; Yen, T.-H.; Tseng, Y.-J.; Hu, C.-H.; Lee, G.-H.; Chiang, M.-H. Electron Delocalization from the Fullerene Attachment to the Diiron Core within the Active-Site Mimics of [FeFe]-Hydrogenase. *Inorg. Chem.* **2012**, *51*, 5997−5999.

(22) Camara, J. M.; Rauchfuss, T. B. Combining Acid−Base, Redox and Substrate Binding Functionalities to Give a Complete Model for the [FeFe]-Hydrogenase. *Nat. Chem.* **2012**, *4*, 26−30.
(23) Becker, R.; Amirjalayer, S.; Li, P.; Woutersen, S.; Reek, J. N. H. An Iron-Iron Hydrogenase Mimic with Appended Electron Reservoir for Efficient Proton Reduction in Aqueous Media. *Sci. Adv.* **2016**, *2*, e1501014.
(24) Li, P.; Amirjalayer, S.; Hartl, F.; Lutz, M.; Bruin, B. d.; Becker, R.; Woutersen, S.; Reek, J. N. H. Direct Probing of Photoinduced Electron Transfer in a Self-Assembled Biomimetic [2Fe2S]-Hydrogenase Complex Using Ultrafast Vibrational Spectroscopy. *Inorg. Chem.* **2014**, *53*, 5373−5383.
(25) Song, L.-C.; Tang, M.-Y.; Mei, S.-Z.; Huang, J.-H.; Hu, Q.-M. The Active Site Model for Iron-Only Hydrogenases Coordinatively Bonded to a Metalloporphyrin Photosensitizer. *Organometallics* **2007**, *26*, 1575−1577.
(26) Li, X.; Wang, M.; Zhang, S.; Pan, J.; Na, Y.; Liu, J.; Åkermark, B.; Sun, L. Noncovalent Assembly of a Metalloporphyrin and an Iron Hydrogenase Active-Site Model: Photo-Induced Electron Transfer and Hydrogen Generation. *J. Phys. Chem. B* **2008**, *112*, 8198−8202.
(27) Kluwer, A. M.; Kapre, R.; Hartl, F.; Lutz, M.; Spek, A. L.; Brouwer, A. M.; van Leeuwen, P. W. N. M.; Reek, J. N. H. Self-Assembled Biomimetic [2Fe2S]-Hydrogenase-Based Photocatalyst for Molecular Hydrogen Evolution. *Proc. Natl. Acad. Sci. U. S. A.* **2009**, *106*, 10460.
(28) Jana, A.; Bähring, S.; Ishida, M.; Goeb, S.; Canevet, D.; Sallé, M.; Jeppesen, J. O.; Sessler, J. L. Functionalised Tetrathiafulvalene-(TTF-) Macrocycles: Recent Trends in Applied Supramolecular Chemistry. *Chem. Soc. Rev.* **2018**, *47*, 5614−5645 and the pertinent references therein..
(29) Jana, A.; Ishida, M.; Park, J. S.; Bähring, S.; Jeppesen, J. O.; Sessler, J. L. Tetrathiafulvalene- (TTF-) Derived Oligopyrrolic Macrocycles. *Chem. Rev.* **2017**, *117*, 2641−2710 and the pertinent references therein..
(30) Hammerich, O.; Nielsen, M. B. Extended Tetrathiafulvalenes with Polycyclic Aromatic Cores. *J. Mater. Chem. C* **2019**, *7*, 2809−2822.
(31) Yamada, J.; Sugimoto, T. *TTF Chemistry: Fundamentals and Applications of Tetrathiafulvalene*; Springer: 2014.
(32) Gorgues, A.; Hudhomme, P.; Sallé, M. Highly Functionalized Tetrathiafulvalenes: Riding Along the Synthetic Trail from Electrophilic Alkynes. *Chem. Rev.* **2004**, *104*, 5151−5184.
(33) Brunetti, F. G.; López, J. L.; Atienza, C.; Martín, N. π-Extended TTF: A Versatile Molecule for Organic Electronics. *J. Mater. Chem.* **2012**, *22*, 4188−4205.
(34) Yamada, H.; Yamashita, M.; Hayashi, H.; Suzuki, M.; Aratani, N. Semiconducting π-Extended Tetrathiafulvalene Derivatives. *Chem. - Eur. J.* **2018**, *24*, 18601−18612.
(35) Ukaj, D.; Bunzen, H.; Berger, J.; Kieslich, G.; Fischer, R. A. Charge-Transfer-Induced Electrical Conductivity in a Tetrathiafulvalene-Based Metal−Organic Framework. *Chem. Mater.* **2021**, *33*, 2532−2542.
(36) Wudl, F.; Smith, G. M.; Hufnagel, E. J. Bis-1,3-dithiolium Chloride: An Unusually Stable Organic Radical Cation. *J. Chem. Soc. D* **1970**, 1453−1454.
(37) Guldi, D. M.; Sánchez, L.; Martín, N. Formation and Characterization of the π-Radical Cation and Dication of π-Extended Tetrathiafulvalene Materials. *J. Phys. Chem. B* **2001**, *105*, 7139−7144.
(38) Ziganshina, A. Y.; Ko, Y. H.; Jeon, W. S.; Kim, K. Stable π-Dimer of a Tetrathiafulvalene Cation Radical Encapsulated in the Cavity of Cucurbit[8]uril. *Chem. Commun.* **2004**, 806−807.
(39) Bigot, J.; Charleux, B.; Cooke, G.; Delattre, F.; Fournier, D.; Lyskawa, J.; Sambe, L.; Stoffelbach, F.; Woisel, P. Tetrathiafulvalene End-Functionalized Poly(N-isopropylacrylamide): A New Class of Amphiphilic Polymer for the Creation of Multistimuli Responsive Micelles. *J. Am. Chem. Soc.* **2010**, *132*, 10796−10801.
(40) Halling, M. D.; Bell, J. D.; Pugmire, R. J.; Grant, D. M.; Miller, J. S. Solid-State NMR Spectra and Long, Intra-Dimer Bonding in the π-[TTF]22+ (TTF = Tetrathiafulvalene) Dication. *J. Phys. Chem. A* **2010**, *114*, 6622−6629.
(41) Sun, W.; Xu, C.-H.; Zhu, Z.; Fang, C.-J.; Yan, C.-H. Chemical-Driven Reconfigurable Arithmetic Functionalities within a Fluorescent Tetrathiafulvalene Derivative. *J. Phys. Chem. C* **2008**, *112*, 16973−16983.
(42) Olaya, A. J.; Ge, P.; Gonthier, J. F.; Pechy, P.; Corminboeuf, C.; Girault, H. H. Four-Electron Oxygen Reduction by Tetrathiafulvalene. *J. Am. Chem. Soc.* **2011**, *133*, 12115−12123.
(43) Olaya, A. J.; Omatsu, T.; Hidalgo-Acosta, J. C.; Riva, J. S.; Bassetto, V. C.; Gasilova, N.; Girault, H. H. A Self-Assembled Organic/Metal Junction for Water Photo-Oxidation. *J. Am. Chem. Soc.* **2019**, *141*, 6765−6774.
(44) Olaya, A. J.; Hidalgo-Acosta, J. C.; Omatsu, T.; Girault, H. H. Photosensitized Hydrogen Evolution on a Floating Electrocatalyst Coupled to Electrochemical Recycling. *J. Am. Chem. Soc.* **2018**, *140*, 10149−10152.
(45) Krishnan, S.; Armstrong, F. A. Order-of-Magnitude Enhancement of an Enzymatic Hydrogen-Air Fuel Cell Based on Pyrenyl Carbon Nanostructures. *Chem. Sci.* **2012**, *3*, 1015−1023.
(46) King, P. W. Designing Interfaces of Hydrogenase−Nanomaterial Hybrids for Efficient Solar Conversion. *Biochim. Biophys. Acta, Bioenerg.* **2013**, *1827*, 949−957.
(47) Watanabe, M.; Honda, Y.; Hagiwara, H.; Ishihara, T. [FeFe]-Hydrogenase and Its Organic Molecule Mimics—Artificial and Bioengineering Application for Hydrogenproduction. *J. Photochem. Photobiol., C* **2017**, *33*, 1−26.
(48) Muñoz, A.; Rodríguez-Pérez, L.; Casado, S.; Illescas, B. M.; Martín, N. Multivalent Fullerene/ π-Extended TTF Electroactive Molecules − Non-Covalent Interaction with Graphene and Charge Transfer Implications. *J. Mater. Chem. C* **2019**, *7*, 8962−8968 and the pertinent references therein..
(49) Stanley, J. L.; Rauchfuss, T. B.; Wilson, S. R. Studies on the Condensation Pathway to and Properties of Diiron Azadithiolate Carbonyls. *Organometallics* **2007**, *26*, 1907−1911.
(50) Moore, A. J.; Bryce, M. R. Highly Conjugated π-Electron Donors for Organic Metals: Synthesis and Redox Chemistry of New 1,3-Dithiole and 1,3-Selenathiole Derivatives. *J. Chem. Soc., Perkin Trans. 1* **1991**, *1*, 157−168.
(51) Martín, N.; Sánchez, L.; Seoane, C.; Fernández, C. Synthesis and Redox Properties of Largely π-Extended p-Quinodimethane Analogues of Tetrathiafulvalene. *Synth. Met.* **1996**, *78*, 137−141.
(52) Cabeza, J. A.; Martínez-García, M. A.; Riera, V.; Ardura, D.; García-Granda, S. Binuclear Iron(I), Ruthenium(I), and Osmium(I) Hexacarbonyl Complexes Containing a Bridging Benzene-1,2-Dithiolate Ligand. Synthesis, X-Ray Structures, Protonation Reactions, and EHMO Calculations. *Organometallics* **1998**, *17*, 1471−1477.
(53) Frisch, M. J.; Trucks, G. W.; Schlegel, H. B.; Scuseria, G. E.; Robb, M. A.; Cheeseman, J. R.; Scalmani, G.; Barone, V.; Petersson, G. A.; Nakatsuji, H.; Li, X.; Caricato, M.; Marenich, A. V.; Bloino, J.; Janesko, B. G.; Gomperts, R.; Mennucci, B.; Hratchian, H. P.; Ortiz, J. V.; Izmaylov, A. F.; Sonnenberg, J. L.; Williams; Ding, F.; Lipparini, F.; Egidi, F.; Goings, J.; Peng, B.; Petrone, A.; Henderson, T.; Ranasinghe, D.; Zakrzewski, V. G.; Gao, J.; Rega, N.; Zheng, G.; Liang, W.; Hada, M.; Ehara, M.; Toyota, K.; Fukuda, R.; Hasegawa, J.; Ishida, M.; Nakajima, T.; Honda, Y.; Kitao, O.; Nakai, H.; Vreven, T.; Throssell, K.; Montgomery, J. A., Jr.; Peralta, J. E.; Ogliaro, F.; Bearpark, M. J.; Heyd, J. J.; Brothers, E. N.; Kudin, K. N.; Staroverov, V. N.; Keith, T. A.; Kobayashi, R.; Normand, J.; Raghavachari, K.; Rendell, A. P.; Burant, J. C.; Iyengar, S. S.; Tomasi, J.; Cossi, M.; Millam, J. M.; Klene, M.; Adamo, C.; Cammi, R.; Ochterski, J. W.; Martin, R. L.; Morokuma, K.; Farkas, O.; Foresman, J. B.; Fox, D. J. *Gaussian 16 Rev. C.01*; Gaussian Inc.: 2016.
(54) Zhao, Y.; Truhlar, D. G. The M06 Suite of Density Functionals for Main Group Thermochemistry, Thermochemical Kinetics, Noncovalent Interactions, Excited States, and Transition Elements: Two New Functionals and Systematic Testing of Four M06-Class


https://doi.org/10.1021/acsorginorgau.1c00011
ACS Org. Inorg. Au 2022, 2, 23−33

Functionals and 12 Other Functionals. *Theor. Chem. Acc.* **2008**, *120*, 215−241.
(55) Zhao, Y.; Truhlar, D. G. Density Functionals with Broad Applicability in Chemistry. *Acc. Chem. Res.* **2008**, *41*, 157−167.
(56) Zhao, Y.; Truhlar, D. G. Applications and Validations of the Minnesota Density Functionals. *Chem. Phys. Lett.* **2011**, *502*, 1−13.
(57) Wheeler, S. E.; Houk, K. N. Integration Grid Errors for Meta-GGA-Predicted Reaction Energies: Origin of Grid Errors for the M06 Suite of Functionals. *J. Chem. Theory Comput.* **2010**, *6*, 395−404.
(58) Andrae, D.; Häußermann, U.; Dolg, M.; Stoll, H.; Preuß, H. Energy-Adjustedab Initio Pseudopotentials for the Second and Third Row Transition Elements. *Theor. Chim. Acta* **1990**, *77*, 123−141.
(59) Ehlers, A. W.; Böhme, M.; Dapprich, S.; Gobbi, A.; Höllwarth, A.; Jonas, V.; Köhler, K. F.; Stegmann, R.; Veldkamp, A.; Frenking, G. A Set of f-Polarization Functions for Pseudo-Potential Basis Sets of the Transition Metals Sc-Cu, Y-Ag and La-Au. *Chem. Phys. Lett.* **1993**, *208*, 111−114.
(60) Hehre, W. J.; Ditchfield, R.; Pople, J. A. Self—Consistent Molecular Orbital Methods. Xii. Further Extensions of Gaussian—Type Basis Sets for Use in Molecular Orbital Studies of Organic Molecules. *J. Chem. Phys.* **1972**, *56*, 2257−2261.
(61) Francl, M. M.; Pietro, W. J.; Hehre, W. J.; Binkley, J. S.; Gordon, M. S.; DeFrees, D. J.; Pople, J. A. Self-Consistent Molecular Orbital Methods. XXIII. A Polarization-Type Basis Set for Second-Row Elements. *J. Chem. Phys.* **1982**, *77*, 3654−3665.
(62) Marenich, A. V.; Cramer, C. J.; Truhlar, D. G. Universal Solvation Model Based on Solute Electron Density and on a Continuum Model of the Solvent Defined by the Bulk Dielectric Constant and Atomic Surface Tensions. *J. Phys. Chem. B* **2009**, *113*, 6378−6396.
(63) Sheldrick, G. M. Crystal Structure Refinement with SHELXL. *Acta Crystallogr., Sect. C: Struct. Chem.* **2015**, *C71*, 3−8.
(64) The procedure to obtain photoadducts **6**−**8** was developed in our laboratories. See: Aguado, S.; Casarrubios, L.; Ramírez de Arellano, C.; Sierra, M. A. Revisiting the Photochemical Synthesis of [FeFe]-Hydrogenase Mimics: Reaction Optimization, Mechanistic Study and Electrochemical Behaviour. *RSC Adv.* **2020**, *10*, 29855−29867.
(65) Rovira, C. Bis(ethylenethio)tetrathiafulvalene (BET-TTF) and Related Dissymmetrical Electron Donors: From the Molecule to Functional Molecular Materials and Devices (OFETs). *Chem. Rev.* **2004**, *104*, 5289−5318.
(66) Baik, M.-H.; Ziegler, T.; Schauer, C. K. Density Functional Theory Study of Redox Pairs. 1. Dinuclear Iron Complexes That Undergo Multielectron Redox Reactions Accompanied by a Reversible Structural Change. *J. Am. Chem. Soc.* **2000**, *122*, 9143−9154.
(67) Totten, L. A.; Roberts, A. L. Calculated One- and Two-Electron Reduction Potentials and Related Molecular Descriptors for Reduction of Alkyl and Vinyl Halides in Water. *Crit. Rev. Environ. Sci. Technol.* **2001**, *31*, 175−221.
(68) Kim, H.; Park, J.; Lee, Y. S. Prediction of the Reduction Potential of Tris(2,2′-bipyridinyl)Iron(III/II) Derivatives. *J. Comput. Chem.* **2015**, *36*, 33−41.
(69) Ghosh, S.; Rahaman, A.; Holt, K. B.; Nordlander, E.; Richmond, M. G.; Kabir, S. E.; Hogarth, G. Hydrogenase Biomimetics with Redox-Active Ligands: Electrocatalytic Proton Reduction by $[Fe_2(CO)_4(\kappa 2\text{-diamine})(\mu\text{-edt})]$ (diamine = 2,2′-bipy, 1,10-phen). *Polyhedron* **2016**, *116*, 127−135.
(70) Collado, A.; Torres, A.; Gómez-Gallego, M.; Casarrubios, L.; Sierra, M. A. A Model for the Prediction of the Redox Potentials in [FeFe]-Clusters from the Electronic Properties of Isocyanide Ligands. *ChemistrySelect* **2020**, *5*, 7177−7182.
(71) Chong, D.; Georgakaki, I. P.; Mejia-Rodriguez, R.; Sanabria-Chinchilla, J.; Soriaga, M. P.; Darensbourg, M. Y. Electrocatalysis of Hydrogen Production by Active Site Analogues of the Iron Hydrogenase Enzyme: Structure/Function Relationships. *Dalton Trans.* **2003**, 4158−4163.
(72) Felton, G. A. N.; Vannucci, A. K.; Chen, J.; Lockett, L. T.; Okumura, N.; Petro, B. J.; Zakai, U. I.; Evans, D. H.; Glass, R. S.; Lichtenberger, D. L. Hydrogen Generation from Weak Acids: Electrochemical and Computational Studies of a Diiron Hydrogenase Mimic. *J. Am. Chem. Soc.* **2007**, *129*, 12521−12530.
(73) Avello, M. G.; de la Torre, M. C.; Sierra, M. A.; Gornitzka, H.; Hemmert, C. Central (S) to Central (M = Ir, Rh) to Planar (Metallocene, M = Fe, Ru) Chirality Transfer Using Sulfoxide-Substituted Mesoionic Carbene Ligands: Synthesis of Bimetallic Planar Chiral Metallocenes. *Chem.-Eur. J.* **2019**, *25*, 13344−13353.
(74) Felton, G. A. N.; Glass, R. S.; Lichtenberger, D. L.; Evans, D. H. Iron-Only Hydrogenase Mimics. Thermodynamic Aspects of the Use of Electrochemistry to Evaluate Catalytic Efficiency for Hydrogen Generation. *Inorg. Chem.* **2006**, *45*, 9181−9184.
(75) Trautwein, R.; Almazahreh, L. R.; Görls, H.; Weigand, W. Steric Effect of the Dithiolato Linker on the Reduction Mechanism of $[Fe_2(CO)_6\{\mu\text{-}(XCH_2)_2CRR'\}]$ Hydrogenase Models (X = S, Se). *Dalton Trans.* **2015**, *44*, 18780−18794.
(76) Abul-Futouh, H.; Skabeev, A.; Botteri, D.; Zagranyarski, Y.; Görls, H.; Weigand, W.; Peneva, K. Toward a Tunable Synthetic [FeFe]-Hydrogenase H-Cluster Mimic Mediated by Perylene Monoimide Model Complexes: Insight into Molecular Structures and Electrochemical Characteristics. *Organometallics* **2018**, *37*, 3278−3285.
(77) Gao, S.; Liang, Q.; Duan, Q.; Jiang, D.; Zhao, J. Electrochemical Proton Reductions in Varying Acidic Media by a Simple Synthetic Hydrogenase Mimic. *Int. J. Hydrogen Energy* **2018**, *43*, 7245−7256.
(78) For complex **6** addition of more than 5.7 equiv of $HBF_4{\cdot}Et_2O$ resulted in solid deposition on the electrode.
(79) It is known that the protonation of exTTF forms $[exTTF]H^+$, considerably lowering the reduction potential. See: Frère, P.; Skabara, P. J. Salts of Extended Tetrathiafulvalene Analogues: Relationships between Molecular Structure, Electrochemical Properties and Solid State Organisation. *Chem. Soc. Rev.* **2005**, *34*, 69−98.
(80) $^1H$ NMR experiments were carried out in $CDCl_3$ on addition of 1 and 11 equiv of $HBF_4{\cdot}Et_2O$. The appearance of two new signals centered at 8.80 ppm was attributed to the protonated form of complex **7**.
(81) Felton, G. A. N.; Mebi, C. A.; Petro, B. J.; Vannucci, A. K.; Evans, D. H.; Glass, R. S.; Lichtenberger, D. L. Review of Electrochemical Studies of Complexes Containing the $Fe_2S_2$ Core Characteristic of [FeFe]-Hydrogenases Including Catalysis by These Complexes of the Reduction of Acids to Form Dihydrogen. *J. Organomet. Chem.* **2009**, *694*, 2681−2699.
(82) Stewart, M. P.; Ho, M.-H.; Wiese, S.; Lindstrom, M. L.; Thogerson, C. E.; Raugei, S.; Bullock, R. M.; Helm, M. L. High Catalytic Rates for Hydrogen Production Using Nickel Electrocatalysts with Seven-Membered Cyclic Diphosphine Ligands Containing One Pendant Amine. *J. Am. Chem. Soc.* **2013**, *135*, 6033−6046.
(83) Capon, J.-F.; Gloaguen, F.; Schollhammer, P.; Talarmin, J. Catalysis of the Electrochemical $H_2$ Evolution by Di-Iron Sub-Site Models. *Coord. Chem. Rev.* **2005**, *249*, 1664−1676.
(84) Capon, J.-F.; Gloaguen, F.; Schollhammer, P.; Talarmin, J. Activation of Proton by the Two-Electron Reduction of a Di-Iron Organometallic Complex. *J. Electroanal. Chem.* **2006**, *595*, 47−52.
(85) Roy, L. E.; Batista, E. R.; Hay, P. J. Theoretical Studies on the Redox Potentials of Fe Dinuclear Complexes as Models for Hydrogenase. *Inorg. Chem.* **2008**, *47*, 9228−9237.
(86) Huynh, M. T.; Wang, W.; Rauchfuss, T. B.; Hammes-Schiffer, S. Computational Investigation of [FeFe]-Hydrogenase Models: Characterization of Singly and Doubly Protonated Intermediates and Mechanistic Insights. *Inorg. Chem.* **2014**, *53*, 10301−10311.
(87) Magnuson, A.; Anderlund, M.; Johansson, O.; Lindblad, P.; Lomoth, R.; Polivka, T.; Ott, S.; Stensjö, K.; Styring, S.; Sundström, V.; Hammarström, L. Biomimetic and Microbial Approaches to Solar Fuel Generation. *Acc. Chem. Res.* **2009**, *42*, 1899−1909.


https://doi.org/10.1021/acsorginorgau.1c00011
*ACS Org. Inorg. Au* 2022, 2, 23−33

(88) Ahmed, M. E.; Dey, S.; Darensbourg, M. Y.; Dey, A. Oxygen-Tolerant $H_2$ Production by [FeFe]-$H_2$ase Active Site Mimics Aided by Second Sphere Proton Shuttle. *J. Am. Chem. Soc.* **2018**, *140*, 12457−12468.
(89) Land, H.; Senger, M.; Berggren, G.; Stripp, S. T. Current State of [FeFe]-Hydrogenase Research: Biodiversity and Spectroscopic Investigations. *ACS Catal.* **2020**, *10*, 7069−7086.
(90) Wang, V. C. C.; Esmieu, C.; Redman, H. J.; Berggren, G.; Hammarström, L. The Reactivity of Molecular Oxygen and Reactive Oxygen Species with [FeFe] Hydrogenase Biomimetics: Reversibility and the Role of the Second Coordination Sphere. *Dalton Trans.* **2020**, *49*, 858−865.
(91) Yang, X.; Darensbourg, M. Y. The Roles of Chalcogenides in $O_2$ Protection of $H_2$ase Active Sites. *Chem. Sci.* **2020**, *11*, 9366−9377.
(92) It can be thought that the observed differences may be due to the fast production of $TTF^{\bullet+}$ in aerobic media in comparison to anaerobic media (see Scheme 1). However, as pointed out by one reviewer, the exTTF reactivity with $O_2$ is questionable, since the diiron complex may be degraded at less reducing potentials. To fully understand this process, the stability of the diiron moiety in the first reduction process should be unambiguously demonstrated, which is outside the scope of this paper. We thank the reviewer for this clever insight, and this problem will be addressed in future work.


https://doi.org/10.1021/acsorginorgau.1c00011
*ACS Org. Inorg. Au* 2022, 2, 23−33